NASA TECHNICAL MEMORANDUM

NASA TM X-1692

NASA TM X-1692



# EFFECT OF POROUS BLEED IN A HIGH-PERFORMANCE AXISYMMETRIC, MIXED-COMPRESSION INLET AT MACH 2.50

*by Robert W. Cubbison, Edward T. Meleason, and David F. Johnson*

*Lewis Research Center*
*Cleveland, Ohio*

NATIONAL AERONAUTICS AND SPACE ADMINISTRATION • WASHINGTON, D. C. • NOVEMBER 1968

NASA TM X-1692

# EFFECT OF POROUS BLEED IN A HIGH-PERFORMANCE AXISYMMETRIC, MIXED-COMPRESSION INLET AT MACH 2.50

By Robert W. Cubbison, Edward T. Meleason, and David F. Johnson

Lewis Research Center
Cleveland, Ohio

NATIONAL AERONAUTICS AND SPACE ADMINISTRATION

For sale by the Clearinghouse for Federal Scientific and Technical Information
Springfield, Virginia 22151 – CFSTI price $3.00

## ABSTRACT

A study to determine the effect of boundary layer bleed location and the amount of total bleed flow on the performance of a mixed-compression, axisymmetric, reflecting-shock inlet was conducted in the Lewis 10- by 10-Foot Supersonic Wind Tunnel at Mach 2.498. Best overall inlet performance was obtained with 2.5 percent supercritical bleed located just downstream of the last cowl and centerbody shock reflection points in the supersonic diffuser. Critical pressure recovery was 0.899 with 16.5 percent distortion, and the subcritical operating range was 7.8 percent of engine corrected airflow. Distortion considerations may dictate either more bleed or use of vortex generators.

# EFFECT OF POROUS BLEED IN A HIGH-PERFORMANCE AXISYMMETRIC, MIXED-COMPRESSION INLET AT MACH 2.50

by Robert W. Cubbison, Edward T. Meleason and David F. Johnson
Lewis Research Center

## SUMMARY

A study has been made of the effects of boundary layer bleed rate and its location on the performance of an axisymmetric inlet designed for Mach 2.5 and with 60 percent of the supersonic area contraction occurring internally. Porous bleed regions were located on the cowl and centerbody in both the supersonic diffuser and in the throat region. The investigation was conducted at Mach 2.498 and $0^{\circ}$ angle of attack. The maximum angle of attack before an unstart occurred was determined. The test Reynolds number (based on inlet capture diameter) was $3.88 \times 10^6$.

The optimum bleed location was determined by moving the supersonic diffuser bleed from just ahead of both the shock reflection point on the cowl and the second shock reflection point on the centerbody to just aft of these points. Total bleed-mass flow ratio was about 0.055 during supercritical operation. As the bleed was moved aft, the overall pressure recovery increased from 0.881 to 0.906 with a constant distortion of 0.14 at critical inlet operation. The subcritical operating range was also increased from 6.8 percent of engine corrected airflow to 8.5 percent. This stable range resulted from a favorable shock-induced boundary layer separation on the centerbody which allowed the terminal shock to move forward of the geometric throat onto the boundary layer bleed regions. The unstart angle of attack during critical operation was reduced from $3.6^{\circ}$ (forward bleed location) to $2.7^{\circ}$ (aft bleed location).

To determine the effect of bleed flow rate, the total supercritical bleed flow was varied from 0.025 (no throat bleed) to 0.095. The pressure recovery at critical operation increased from 0.899 to 0.949 and the distortion decreased from 0.165 to 0.057 as the critical bleed mass-flow ratio increased from 0.025 to 0.145. Large increases in total supercritical bleed flow significantly reduced the subcritical operating range of the inlet. The maximum unstart angle of attack of $2.7^{\circ}$ was unchanged with increased bleed capability. However, the unstart angle at minimum stable operation increased from $0.2^{\circ}$ to $2.6^{\circ}$.

The effects of bleed location and amount of bleed on the payload characteristics of a typical supersonic transport configuration were determined. Generally, the downstream bleed location exhibited a significant improvement in payload over the other locations at all operating conditions. With the inlet operating at a 7 percent stability margin, the improvement in payload was 10.5 passengers compared to the upstream location. The mission analysis further indicated that the least amount of bleed provided the best payload capability; however, the distortion levels may be too high without vortex generators.

# INTRODUCTION

To date, very little information has been published about the inlet-engine dynamics of a complete airbreathing propulsion system operating at supersonic speeds. In order to investigate this area and the associated control problems, an experimental program is being conducted in the Lewis 10- by 10-Foot Supersonic Wind Tunnel. For the initial tests, an axisymmetric inlet was selected with a design Mach number of 2.5 and with 60 percent of the supersonic area contraction occurring internally. This report presents the results of the boundary layer bleed development for this inlet which was conducted prior to its use with an engine.

To achieve the desired high level of inlet performance, it is necessary to minimize the effect of shock-boundary layer interactions in the inlet. In the supersonic diffuser of a reflecting shock inlet, this control is generally achieved by maintaining shock wave pressure rises below separation values and by locating bleed zones in the vicinity of the shock impingement points on the diffuser surfaces. Because of bleed drag penalties, the amount of flow removed should be minimized. The location of the bleed regions relative to the shock impingement points can influence the amount of bleed required to provide adequate boundary layer control. Shock-boundary layer interaction studies with bleed on a flat plate in reference 1 indicate that bleed should be located upstream of a shock reflection point on the basis of producing the theoretical pressure rise across the incident and reflected shock. However, when overall inlet performance is considered, other factors may also influence the choice of bleed location. For mixed-compression inlets, subcritical stability margins on the order of 7 percent of engine corrected airflow are required to avoid inlet unstart from such things as afterburner hard-light or sudden throttle advance. Location and amount of bleed can influence the performance penalties resulting from operation at these stability margins. A brief mission analysis for a typical supersonic transport is included to assess the cost of these penalties in terms of passengers. Another area of considerable importance, which can also be influenced by the amount of bleed and its location, is the tolerance of the inlet to yaw and angle-of-attack effects without incurring inlet unstart.

The purpose of the present cold-pipe investigation was to evaluate several bleed locations (relative to the shock impingement points) and bleed flow rates to determine their effectiveness in achieving high inlet performance. Flow surveys were made at points ahead of the throat, just downstream of the throat region, midway in the subsonic diffuser, and at the diffuser exit. For engine matching, diffuser exit performance levels of at least 90 percent total pressure recovery with 10 percent distortion or less were desired.

The test was conducted in the Lewis 10- by 10-Foot Supersonic Wind Tunnel at Mach 2.498 and a Reynolds number of $3.88 \times 10^6$ based on cowl lip diameter. In addition to the

flow surveys, measurements were also made of inlet and bleed flow rates, total pressure recovery, and engine face distortion. The maximum angle of attack before an inlet unstart occurred was also determined.

## SYMBOLS

| | |
|---|---|
| $A$ | flow area |
| $A_c$ | capture area, 0.1758 $m^2$ |
| $b$ | vortex generator height, 1.27 cm |
| $M$ | Mach number |
| $m/m_0$ | mass-flow ratio |
| $P$ | total pressure |
| $\frac{P_{max}-P_{min}}{P_{av}}$ | distortion parameter |
| $p$ | static pressure |
| $R_c$ | inlet capture radius, 0.2366 m |
| $r$ | radius |
| SI | stability index, $\left[1 - \frac{\left(\frac{w\sqrt{\theta}}{\delta}\right)_{5,\,min\ stable}}{\left(\frac{w\sqrt{\theta}}{\delta}\right)_5}\right] \times 100$ |
| $T$ | total temperature |
| $w$ | weight flow rate |
| $x$ | axial distance from spike tip |
| $\alpha$ | angle of attack |
| $\Delta$ | increment |
| $\delta$ | $P/10.131\times10^3$ $N/m^2$ |
| $\theta$ | $T/288.2$ K |
| $\theta_l$ | cowl-lip-position parameter, $\tan^{-1}\frac{1}{(x/R_c)_l}$ |

Subscripts:

| | |
|---|---|
| av | average |
| BL | bleed |
| e | exit |
| $l$ | cowl lip |
| max | maximum |
| min | minimum |
| min stable | minimum stable inlet operating point |
| un | unstart |
| x | local |
| 0 | free stream |
| 5 | diffuser exit station |

## APPARATUS AND PROCEDURE

The inlet used in this investigation was an axisymmetric mixed-compression type designed for Mach 2.50 with a translating centerbody to effect an inlet start. At the design Mach number, 40 percent of the supersonic flow area contraction was external and 60 percent was internal. The inlet was attached to a cylindrical nacelle 0.635 meters in diameter in which either a J-85/13 engine or a cold-pipe choked-exit plug assembly could be installed. For this study, only the cold pipe was used. Figure 1 is a photograph of the inlet-nacelle combination mounted from a vertical strut in the wind tunnel test section.

At the design Mach number of 2.50 and a free-stream temperature of 390 K, the inlet was sized to match J-85/13 engine corrected airflow requirements of 15.83 kilograms per second with 88.6 percent of the capture mass flow at a total pressure recovery of 90 percent. This resulted in an inlet capture area of 0.1758 square meters. Of the remaining inlet flow, 6 to 7 percent was allotted for performance bleed, 4 percent for engine and ejector cooling air, and the rest used through the overboard bypass for terminal shock position control. Total pressure distortion at the engine face of 10 percent or less was desired at the design conditions.

Some elements of the inlet aerodynamic design are presented in figure 2. External compression was accomplished with a $12.5^{\circ}$ half-angle cone which remained conical to a point 2.88 cowl lip radii from the tip. At design conditions the spike tip oblique shock

passed just ahead of the cowl lip so that approximately 0.25 percent of the capture airflow was spilled over the lip. Internal contours and flow conditions in the supersonic diffuser were computed by the method of reference 2. The initial internal cowl lip angle of $0^{o}$ generated an internal shock which reflected twice before reaching the throat. In addition, isentropic compression was also included. Theoretical shock impingement points were at ratios of longitudinal distance to cowl lip radius ($x/R_c$) of 2.88 and 3.475 on the centerbody and 3.25 on the cowl. The pressure rise across individual shock reflection points was maintained at values less than those causing separation of a turbulent boundary layer. An inlet with similar supersonic diffuser design has been studied at Mach 3.0 and is reported in reference 3.

The geometric throat was located at $x/R_c = 3.475$ (centerbody surface), where the theoretical average supersonic Mach number was 1.239 with a total pressure recovery of 0.988. Behind the terminal shock, the theoretical recovery was 0.975 at a Mach number of 0.8125. At the geometric throat, the centerbody turned sharply from an angle of about $0^{o}$ to $-5.7^{o}$, leading to a $1^{o}$ equivalent conical expansion throat region. The throat region length was 4 hydraulic radii. The remainder of the subsonic diffuser was designed as an $8^{o}$ equivalent conical expansion. The required subsonic diffuser length using this criteria was 3.5 cowl lip radii. However, additional length was required due to overboard bypass exit requirements. The resulting total length from cone tip to compressor face was 7.72 cowl lip radii. Figure 2(b) shows the internal area distribution through the inlet for the Mach 2.50 design case.

Additional details of the inlet design are shown in figures 3(a) and (b). The aft portion of the subsonic diffuser contained three hollow centerbody support struts which divided the duct into three compartments back to the engine face. Provisions were also included for installing vortex generators on the cowl and centerbody aft of the throat region at an $x/R_c$ of 4.145. Only one bleed configuration presented in this report had vortex generators installed, and these were on the centerbody only. Details of this generator configuration are shown in figure 3(c). The inlet design also included provisions for two bypass systems: a high response overboard system for shock position control, and a low speed valve to control secondary flow through the nacelle for engine and ejector cooling. Both bypasses were sealed for the bleed study presented in this report.

Boundary layer properties were investigated after the internal shock reflection points on the cowl and centerbody by rakes at stations 1 and 2 (fig. 3(b)). Rakes in the subsonic diffuser aft of the throat region (station 3), at the subsonic diffuser midpoint (station 4), and at the diffuser exit (station 5) were used to determine local flow profiles. The rakes were circumferentially indexed to avoid mutual interference effects. The overall diffuser exit total pressure recovery was determined from rakes 1-6 (fig. 3(d)) which were area weighted. Additional measurements (rakes 7 to 10) were included in the distortion calculations and in plotting total pressure contours. Static pressure distributions along the

top centerline of both cowl and centerbody were also measured.

The diffuser exit or engine mass-flow ratio was calculated using a calibrated choked plug and an average of eight static pressures in the cold pipe located 4.3 cowl lip radii ahead of the plug exit. Cowl bleed flow rates at both stations were determined from a measured static and total pressure at their respective exits and the measured exit areas (see fig. 3(b)). Flow from the combined centerbody bleed regions was calculated from the pitot-static measurements of the rake in the centerbody cavity just ahead of the support struts. Bleed exit total pressure recoveries were used to compute a bleed drag used in a payload comparison that will be discussed later.

To minimize the shock boundary layer interaction, the inlet design included four porous bleed regions shown schematically in figures 3(a) and (b). These areas were composed of holes 0.3175 centimeters in diameter and drilled normal to the surfaces in circumferential rows. Alternate rows were staggered for a more uniform open area distribution. The maximum distance between hole centers was 0.4763 centimeter. The porous pattern and the amount of bleed in these areas could be altered by filling selected holes. The bleed regions in the supersonic diffuser were located on the cowl and centerbody with respect to the theoretical shock impingement points as shown in figure 4. Also included are the experimentally-determined cowl and second centerbody impingement points. The actual impingement points were determined from measurements of an additional static pressure tube which was located in successive rows of bleed holes for successive tests until the shock impingement point was indicated. The indicated location is accurate to within the distance between rows of bleed holes (0.414 cm). The forward cowl bleed region consisted of twelve rows of holes on the cowl surface between $x/R_c$ values of 3.12 and 3.32. The forward centerbody bleed zone consisted of eight rows of holes on the centerbody surface between $x/R_c$ values of 3.31 and 3.45. Aft bleed areas were located in the throat region in the vicinity of the terminal shock during normal operation. As shown in figure 4, these regions were made up of four rows on the cowl surface and five rows on the centerbody.

The cowl bleed flow was discharged overboard through exits shown in figure 3(b) which have a $15^{\circ}$ discharge angle relative to the external surface. The fore and aft centerbody bleed flows were combined into one plenum and ducted through the hollow centerbody support struts to $30^{\circ}$ louvered exits on the cylindrical portion of the nacelle. All exit areas were sized large enough to insure choking of the bleed holes. In addition, the centerbody exit was located on the cylindrical portion of the nacelle to provide as much pumping action as possible.

The different bleed configurations shown in figure 4 were formed by filling selected rows of holes to control both the amount of bleed and also the location of this bleed with respect to the experimental shock impingement points. The experimental internal shock structure was displaced forward relative to the theoretical location due to the action of

the thick boundary layer at the initial shock reflection point on the centerbody. The first set of bleed configurations were designed to study the effect of bleed location in the supersonic diffuser. These three configurations were identified as: (a) bleed located upstream of the shock impingements (U.S.); (b) bleed located across the shock impingements (A.S.); and (c) bleed located downstream of the shock impingements (D.S.). All three configurations used similar throat bleeds. After determining the downstream bleed locations were more efficient for this inlet, a second set of configurations were designed for optimizing the amount of bleed. Four configurations were tested. Configuration A, which did not have any throat bleed, was the minimum bleed configuration. Configurations B (identical to configuration D.S.) and C provided intermediate amounts of bleed flow. Configuration D provided the maximum amount of bleed tested in the inlet.

## RESULTS AND DISCUSSION

The results of the investigation will be discussed in three parts: first, the effect of bleed location in the supersonic diffuser; second, the effect of the amount of bleed on the inlet performance; and third, the effect of bleed on the payload capability of a typical supersonic transport.

### Effect of Bleed Location

The porous boundary layer bleed in the supersonic diffuser was moved, in relation to the experimentally-determined shock reflection points, from just upstream (configuration U.S.) to across (A.S.) to downstream (D.S.). The porosity was changed to maintain about constant supercritical bleed flow at all three locations. Additional bleed in the throat region was also included.

The effect of bleed location on the variation of peak inlet performance with the cowl-lip-position parameter, $\theta_l$, is shown in figure 5. Except for a general increase in the performance level due to bleed location, all three configurations show little variation in recovery and mass flow between the design $\theta_l$ ($26.47^\circ$) and the shock-on-lip position ($26.72^\circ$). The distortion level increased 0.015 for configuration U.S., remained constant for A.S., and decreased 0.015 for D.S. as $\theta_l$ was increased from design to the shock-on-lip value.

Overall performance of configurations U.S., A.S., and D.S. with a $\theta_l = 26.6^\circ$ is presented in figure 6. As the bleed was moved aft, pressure recovery at critical operation (terminal shock at geometric throat) increased from 0.881 to 0.906 with a constant distortion level of about 0.140. Critical bleed mass-flow ratio was about 0.06, and

supercritically the total bleed was 0.055 for all three configurations. All three bleed configurations exhibited sizable subcritical operating ranges between critical and peak performance conditions. The aft location provided the greatest range. In terms of engine corrected airflow, it was 8.5 percent. Configurations A.S. and U.S. provided lower stability margins of 8.1 and 6.8 percent, respectively. The angle of attack at which the inlet unstarted is also shown on figure 6 for different inlet-operating conditions. Reducing the pressure recovery from peak inlet operation increased the unstart angle of attack ($\alpha_{un}$) until a maximum value was reached. Further decrease in inlet-operating level had no effect on the maximum unstart angle of attack. Moving the supersonic diffuser bleed aft (configuration U.S. to D.S.) reduced the $\alpha_{un}$ at peak inlet operation from $1.1^{o}$ to $0.2^{o}$ and maximum $\alpha_{un}$ from $3.6^{o}$ to $2.7^{o}$.

The performance curves (fig. 6) of configurations A.S. and D.S. showed a region of minor terminal shock instability near a mass-flow ratio of 0.91. This occurred when the terminal shock (moving on the porous cone surface ahead of the geometric throat) caused the boundary layer ahead of the bleed to separate. Further shock movement forced the separation forward. Evidence of this separation will be presented in later figures. Although not apparent on the figure, the centerbody boundary layer aft of the forward bleed in configuration U.S. separated when the terminal shock was just ahead of the geometric throat. Again the separation moved forward as the shock moved forward. This separation apparently reattached due to the action of the bleeds and did not seriously affect the overall performance.

The cowl and centerbody static pressure distributions for configuration D.S. are presented in figure 7. These are typical of the three configurations. The data show that the normal shock can be positioned well ahead of the geometric throat. The most forward location was at an $x/R_c$ of about 3.4 and 3.25 on the centerbody and cowl surfaces, respectively. In this position, the shock was condensed into a plane wave. Separation of the boundary layer ahead of the forward centerbody bleed location that was mentioned earlier was evident from the pressure rises noted at $x/R_c$ values of 3.30 and 3.33. This pressure rise corresponds to a two-dimensional separation wedge angle of $11^{o}$ which agrees reasonably well with the angle that would be predicted from reference 4. With the terminal shock ahead of the geometric throat, this separation apparently induces a high recovery oblique shock system. An idealized sketch of this basic shock system is shown in figure 3. The indicated shock pattern results in an overall pressure recovery higher than would be theoretically predicted from the terminal shock intersecting the final oblique wave ahead of the throat in the design shock structure (fig. 2(a)). Thus, in contrast to what might be expected, this separation proved quite beneficial. The static pressures in the common centerbody bleed plenum were lower than the cone surface values; therefore, it can be concluded that the separation was due to shock-boundary layer interaction and not to recirculation of centerbody bleed from the aft region into the

forward region. Since this separation is a boundary-layer phenomena, which is a function of Reynolds number, it is not clear whether similar results would occur in larger scale versions of this inlet operating at different Reynolds numbers. At critical operation (design point), there was no evidence of this separation. Subcritically (shock ahead of the throat), it occurred in all configurations. As a result, the forward centerbody bleed flow increased which, in turn, permitted further upstream movement of the terminal shock until (as will be shown later) the forward cowl bleed was also affected. The net result was the subcritical operating range shown in figure 6.

Local total pressure profiles at various stations in the diffuser are presented in figures 9(a) and (b) for critical and peak operating conditions, respectively. The centerbody boundary layer at station 1 (behind the first centerbody reflection point) was well behaved; however, it was quite thick, about 10 percent (0.118 cm) of the local annulus height, indicating that bleed in this region may be helpful. At critical operating conditions (fig. 9(a)) measurements at station 2 indicated that all three forward cowl locations appeared equally effective in controlling the boundary layer. However, at peak-operating conditions (fig. 9(b)), configuration D.S. obviously provided the best boundary layer control. Measurements near the centerbody surface at stations 3, 4, and 5 indicate the aft bleed location (D.S.) provided the most effective centerbody boundary layer control. Both configuration U.S. and A.S. indicated the flow bridged the centerbody contour near station 4 at critical (fig. 9(a)) and for supercritical operation (data not shown). With configuration D.S., this bridging was eliminated; however, the profile indicated further improvement from more boundary layer control may be possible. The profiles shown at station 5 in this analysis are for rake 7 (fig. 3(c)). As will be seen later on total pressure contour maps, the pressure levels near the centerbody on this particular rake are the lowest of the diffuser exit rakes.

Because the design average throat Mach number was as low as 1.239, a simple shock reflection at the second centerbody impingement point is not possible unless the centerbody is turned at this point to either weaken or cancel the shock. Since the shock actually impinged ahead of the design point, a Mach reflection should occur. The much lower pressure in the profile near the centerbody at station 3 (fig. 9(a)) indicated the possible presence of this reflection. Locating the bleed across or downstream of the experimental reflection point apparently modified the wall boundary characteristics in a manner similar to the action of a perforated wall in a transonic wind tunnel.

In contrast to the findings of reference 1, the results shown in figure 9 indicate that locating the bleeds downstream of the shock reflection points yielded the best overall performance in this inlet. Increasing the amount of bleed at these locations or perhaps providing bleed capability at the first shock reflection point on the cone surface could further improve the overall performance.

The low pressure measured out in the stream (stations 3 and 4, fig. 9(b)) can be traced to the region between the intersections of the cowl reflected shock and the centerbody boundary-layer separation induced shock with the terminal shock. This region (A) is indicated on figure 8. The resulting total pressure level was approximately that expected from a normal shock at the supersonic Mach number at this point in the diffuser (fig. 2(a)). As the terminal shock was moved aft towards the geometric throat, the radial location of the low pressure moved toward the centerbody. The combination of station 3 and 4 profiles and the centerbody static pressure measurements were used to determine the region of separation on the centerbody ($x/R_c = 3.19$ for peak operation, fig. 7(b)).

The compressor face total pressure contours for critical and peak operation are shown in figures 10(a) and (b), respectively. Because of symmetry, only one-third of the duct is shown. Moving the bleed aft generally reduced the distortion; however, the basic pattern was not changed. Pressure levels were high along the strut surface and in the corners indicating good quality flow in these areas. High pressure lobes form in the middle of the duct primarily near the struts at critical operation. This tendency also appeared at peak operation. At both operating conditions, it was probably a result of the pinching action caused by the lower energy lobe near the surface of the centerbody. This distribution was due to the channeling effect caused by the struts.

Variations of forward cowl, aft cowl, and centerbody bleed flows with overall pressure recovery shown in figure 11 indicate that the supercritical bleed was about the same in all three configurations. The major difference was in the forward cowl of configuration U.S. Although an additional 0.5 percent bleed was removed, the station 2 pressure measurements (fig. 9(a)) showed boundary layer control comparable to configuration A.S. and D.S. At equal bleed flows, configuration D.S. produced equal or higher recovery than the other configurations. The increase in bleed flow as peak pressure recovery was approached was a result of the shock pressure rise moving forward onto the bleed zones.

## Effect of Bleed Amount

Basically the different configurations (fig. 4) studied in this portion of the investigation are modifications of configuration D.S. Configuration B is identical to the configuration designated D.S. in the prior section of this report. The total supercritical bleed capability was increased from 2.5 percent of capture mass flow in configuration A (identical to configuration B but without throat bleed) to 9.5 percent in configuration D which had the maximum porosity available in the throat region and downstream of the reflected shock impingement points.

Variation of peak inlet performance with $\theta_l$ for the various bleed configurations is shown in figure 12. Except for a general increase in the performance level due to in-

creased bleed, all four configurations showed little variation in recovery, mass flow ratio and distortion between design $\theta_l$ ($26.47^{\circ}$) and the shock-on-lip position ($26.72^{\circ}$).

Overall performance of configurations A, B, C, and D is presented in figure 13. Critical pressure recovery was increased from 0.899 to 0.949 as the bleed was increased from 0.025 to 0.145 (configurations A to D). The distortion decreased from 0.165 to 0.057. Configuration D had centerbody vortex generators which would also reduce the distortion. However, the trend from configurations A through C indicates that the major reductions came from the increased bleed. The pressure recovery would also be affected by the generators, but an $8^{\circ}$ equivalent cone diffuser is reasonably efficient; therefore, the effect should be detrimental. Large increases in bleed improved $\alpha_{un}$ from $0.2^{\circ}$ to $2.6^{\circ}$ at peak inlet operation. Maximum $\alpha_{un}$ of about $2.7^{\circ}$ is affected only by the location of the forward bleeds as shown on figure 6. Configuration C, which had an A.S. orientation of the forward cowl bleed, also demonstrated this. As also shown in figure 13, increasing the amount of throat bleed beyond that of configuration B reduced the subcritical operating range of the inlet. Previously it was noted that the subcritical operating range was a result of the terminal shock movement ahead of the geometric throat. By comparing duct static pressure distributions at critical and peak operation (figs. 14(a) and (b), respectively) it can be seen that in the present inlet configutaion, increasing the bleed restricted this movement. As a result, the subcritical operating range of 7.8 percent and 8.5 percent in engine corrected airflow for configutation A and B, respectively, was reduced to 2.8 percent and 1.7 percent for configurations C and D. The apparent reason for the restricted shock movement was found by comparing the centerbody bleed plenum static pressures (near the forward porous surface) to the local cone surface values. For configurations A and B, the ratio of these pressures (data not shown) was about the same indicating about equal bleed flows being removed through the forward centerbody bleed. Increasing the aft centerbody porosity from configuration B to C decreased the pressure ratio across the forward bleed region; consequently, less flow was removed. For configuration D (maximum porosity tested), the pressure ratio was reduced to less than 1.0 indicating some recirculation from the aft region to the forward region at critical inlet operation. At peak, the pressure ratio was slightly greater than 1.0 indicating only a very small amount of forward bleed. The reductions in bleed through the forward centerbody in configurations C and D were due to increasing the bleed capability in the high pressure aft throat region of the centerbody. The recirculation was due to a combination of the large aft bleed and the low surface pressure in the forward bleed region ($x/R_c = 3.42$, fig. 14(a)). Individual compartmentation of the forward and aft centerbody bleed regimes would prevent this loss of forward bleed effectiveness in configurations C and D. Consequently, the subcritical operating range of these two configurations would increase. However, compartmentation of these bleed systems in an axisymmetric translating centerbody inlet introduces additional mechanical complexity.

In the case of configurations A and B, compartmentation would not be expected to increase the stable range.

Effects of increased bleed on diffuser flow profiles are shown in figure 15(a) for critical inlet operation and in figure 15(b) for peak operation. Significant improvements were indicated at all subsonic diffuser stations, especially at critical operation. Configuration C, which had an A.S. orientation of the forward cowl bleed, illustrates the sensitivity at peak operation to bleed location. With configuration D, the profiles at station 5 were exceptionally flat. The improvement near the centerbody was due, in part, to the use of centerbody vortex generators. The general flattening of the cowl side profile was characteristic of increased bleed. The amount of bleed required to make these improvements can be costly in terms of drag.

Increasing the bleed improved the distortion and tended to flatten the low-pressure hump on the centerbody. Compressor face total pressure maps at critical and peak operation (fig. 16(a) and (b), respectively) show the spread from low to high pressure was reduced throughout the duct as the increased bleed removed more of the existing low-energy air in or ahead of the throat region. Large increases in bleed prevented the lobes from forming in mid duct near the strut walls as a result of flattening the low-pressure hump along the centerbody. The vortex generators of configuration D changed the general shape because the resulting vortices swept the low-energy air off of the centerbody surface and up into the duct.

The amounts of bleed flow removed at the forward and aft cowl bleed zones and from the centerbody are shown in figure 17. General increases in level between configurations were due to increased porosity. Because of reduced terminal shock movement in configurations C and D, the forward cowl bleed was not influenced by the shock position as were configurations A and B. Increases in the aft cowl and centerbody bleed rates for inlet pressure recoveries above about 0.90 were due to the terminal shock influence. For configuration D, nearly all of the increased centerbody flow was in the aft region because of the large bleed capability in the high pressure aft region relative to that of the bleed zone ahead of the terminal shock.

## Effect of Bleed on Payload Capability of Typical Supersonic Transport

As discussed in reference 5, the inlet parameters that affect the inlet performance during supersonic cruise will probably have a greater effect of payload than will inlet parameters that are considered during other phases of the mission. During cruise, it is desirable to operate at the maximum payload condition. However, it is also desirable to have sufficient stability margin to minimize the possibility of an inlet unstart due to a sudden throttle advance or afterburner hard-light. Disturbances such as these usually

require stability margins on the order of 7 percent in engine corrected airflow. To assess the penalty involved in operating the various bleed configurations (location and amount) over a range of stability margins, the change in payload resulting from a trade-off between bleed flow rate and inlet recovery was calculated. This payload change in terms of passengers was calculated using the results of an unpublished Mach 2.7 supersonic transport mission study similar to that reported in reference 5 for a Mach 3 aircraft. This analysis assumed a 208-passenger aircraft with a total range of 6480 kilometers. These results indicate a 0.01 change in recovery and bleed drag coefficient produces a passenger change of 4.05 and 4.75, respectively. The reference point (zero $\Delta$ passengers) was assumed to be at 90 percent pressure recovery with a bleed drag coefficient of 0.035. Pressure recovery data of figures 6 and 13 were used to determine the effect of recovery variations for the various bleed locations and amounts of bleed, respectively. The respective bleed drag coefficients (based on inlet capture area) were calculated from the measured bleed exit total pressure recoveries presented in figures 18(a) and (b) and flow rates from figures 11 and 17 assuming a sonic axial discharge. The stability index is defined as the percentage change in engine corrected airflow between any given operating condition and the minimum stable point just prior to unstart.

The payload penalties in terms of passengers for the three bleed locations (configurations U.S., A.S., and D.S.) incurred by operating at various stability margins are presented in figure 19. Generally, at all operating conditions configuration D.S. showed a significant improvement in payload over the other configurations. For example, at 7 percent stability index, the improvement in payload was 10.5 passengers compared to configuration U.S. The distortion level was unchanged. This improvement was due to the increase in overall recovery for a given bleed flow. For these configurations, the desired stability margin of 7 percent was obtained with the inlet operating with the terminal shock near the geometric throat or design position.

The payload penalties involved by varying the amount of supercritical bleed (configurations A, B, C, and D) are presented in figure 20. In general, configuration A provided the best performance; however, vortex generators may be required to reduce the distortion. At the desired 7 percent stability margin, increasing the bleed from 2.5 to 11.5 percent of capture mass flow (configurations A to D) cost 11.5 passengers. For configurations A and B, the desired stability occurred with the terminal shock near the geometric throat (design point). Further increases in bleed (configurations C and D) resulted in the terminal shock being positioned progressively further downstream of the design point to achieve the desired stability margin. Again, this was due to reduced forward centerbody bleed effectiveness in configurations C and D resulting from noncompartmentation of the bleed plenum.

# SUMMARY OF RESULTS

A cold-pipe investigation was conducted to study the effect of bleed location and the amount of boundary layer control bleed on an axisymmetric, mixed-compression inlet designed for Mach 2.5. A $12.5^{\circ}$ half-angle cone provided the external compression. Sixty percent of the overall supersonic area contraction occurred internally. The internal compression was accomplished by isentropic compression combined with two reflections of the cowl-lip oblique shock. The performance of the inlet was sensitive to the bleed location relative to the impingement points on the centerbody and cowl surfaces of the cowl-lip shock reflections. Moving the bleeds from forward to aft of the shock impingement points produced the following results:

1. At critical operation, the inlet overall recovery increased from 0.881 to 0.906 and the distortion remained constant at about 0.14. The bleed mass-flow ratios were about 0.06 and 0.055 for critical and supercritical operation, respectively.

2. The aft bleed location provided the greatest subcritical stability margin of about 8.5 percent in engine corrected airflow, which decreased to 6.8 percent as the bleed was moved forward. This sizable subcritical operating range resulted from a favorable shock-induced boundary-layer separation on the centerbody which allowed the terminal shock to move forward of the geometric throat.

3. The maximum angle of attack before an unstart occurred was reduced from $3.6^{\circ}$ to $2.7^{\circ}$ as the bleed was moved from forward to aft of the reflected shock impingement points. At peak inlet operating conditions, the maximum angle of attack was reduced from $1.1^{\circ}$ to $0.2^{\circ}$.

With the supersonic diffuser bleed located just aft of the cowl and the centerbody shock impingement points, the total supercritical bleed flow was increased from 2.5 percent (zero throat bleed) to 9.5 percent with the following results:

1. Critical overall pressure recovery increased from 0.899 to 0.949 with significant reductions in distortion from 0.165 to about 0.057 as the bleed increased from 0.025 to 0.145.

2. Large amounts of bleed substantially reduced the inlet subcritical operating range of 7.8 percent engine corrected airflow. This was due to reduced forward centerbody bleed effectiveness resulting from noncompartmentation of the bleed plenum.

3. Maximum angle of attack prior to an unstart (about $2.7^{\circ}$) was unaffected by increased throat bleed; however, the unstart angle at peak inlet operating conditions increased from about $0.2^{\circ}$ to $2.6^{\circ}$.

The effects of bleed location and amount of bleed on the payload characteristics of a typical supersonic transport configuration were determined with the following results:

1. At all operating conditions, the aft bleed location exhibited a significant improvement in payload. At a 7 percent stability margin, the improvement in payload was 10.5 passengers compared to the upstream bleed location.

2. For all three bleed locations, a 7 percent stability margin was achieved with the terminal shock located near the design position (geometric throat).

3. The least amount of bleed (0.025 of capture mass flow ratio supercritically) provided the best payload capability. However, the distortion levels may dictate additional bleed or vortex generators. At a 7 percent stability margin, increasing the supercritical bleed up to about 11.5 percent cost 11.5 passengers.

4. To achieve the desired 7 percent stability margin with the large bleed configurations in this inlet, it was necessary to operate with the terminal shock downstream of its design position (geometric throat).

Lewis Research Center,
National Aeronautics and Space Administration,
Cleveland, Ohio, June 25, 1968,
126-15-02-11-22.

## REFERENCES

1. Strike, W. T.; and Rippy, J. O.: Influence of Suction on the Interaction of an Oblique Shock with a Turbulent Boundary Layer at Mach Number 3.0. Rep. AEDC-TN-61-129, Arnold Eng. Development Center, Oct. 1961.

2. Sorensen, Virginia L.: Computer Program for Calculating Flow Fields in Supersonic Inlets. NASA TN D-2897, 1965.

3. Sorensen, Norman E.; and Smeltzer, Donald B.: Investigation of a Large-Scale Mixed-Compression Axisymmetric Inlet System Capable of High Performance at Mach Numbers 0.6 to 3.0. NASA TM X-1507, 1968.

4. Nussdorfer, T. J.: Some Observations of Shock-Induced Turbulent Separation on Supersonic Diffusers. NACA RM E51L26, 1954.

5. Koenig, Robert W.: Inlet Sensitivity Study for a Supersonic Transport. NASA TN D-3881, 1967.

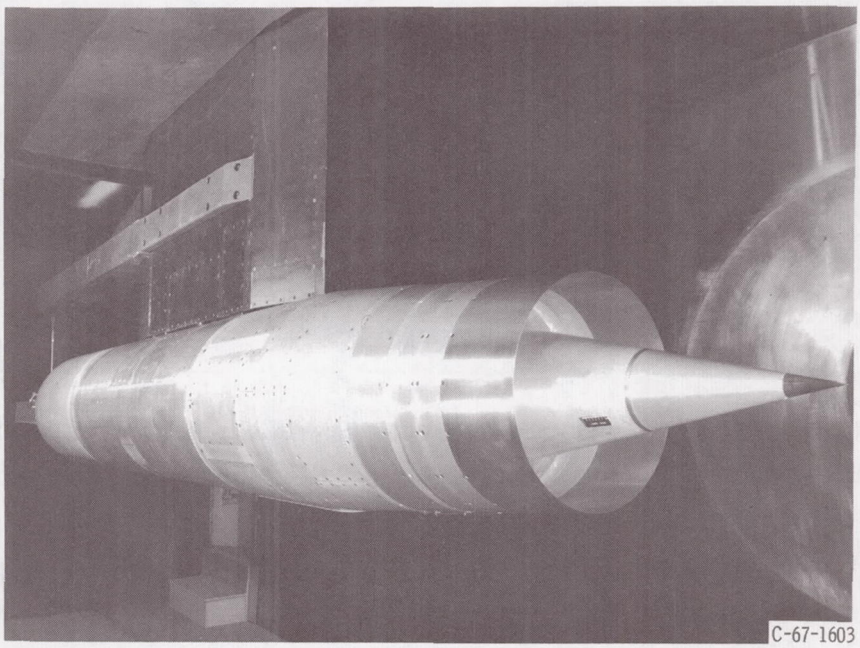


Figure 1. - Mixed-compression inlet model installed in 10- by 10-foot Supersonic Wind Tunnel.

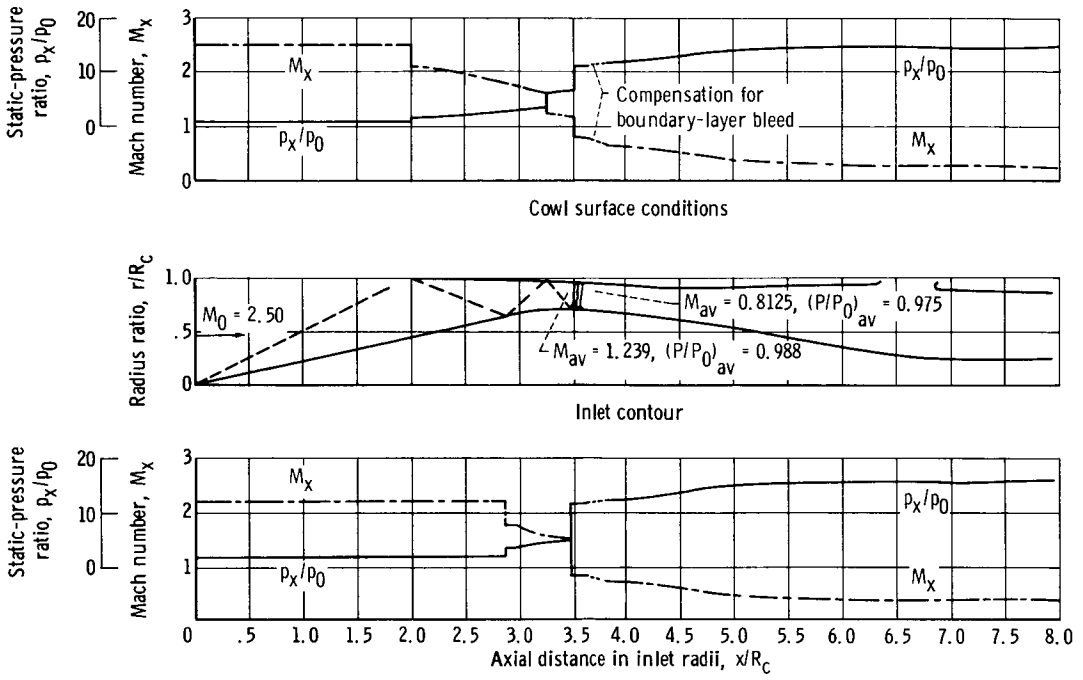


(a) Inlet dimensions and theoretical flow conditions.

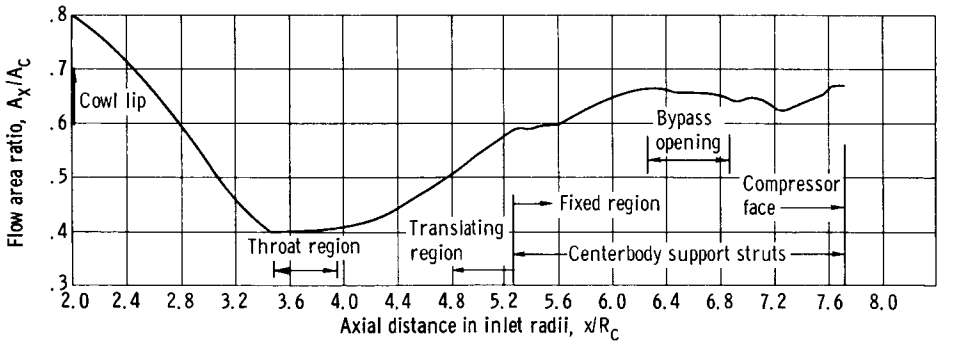


(b) Diffuser area variation for $\theta_l = 26.72°$.

Figure 2. - Aerodynamic details.

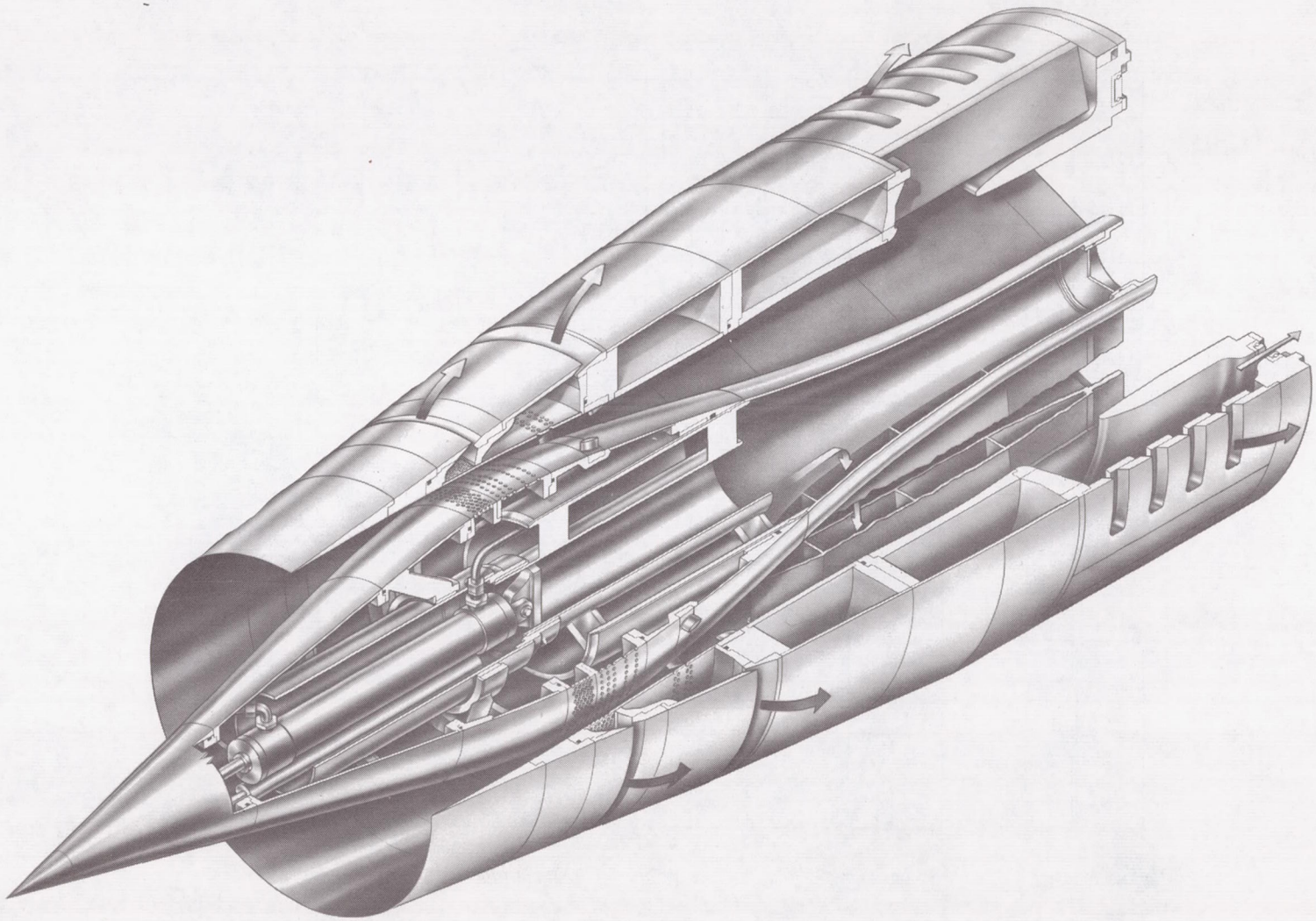

(a) Isometric view of inlet.

Figure 3. - Model details

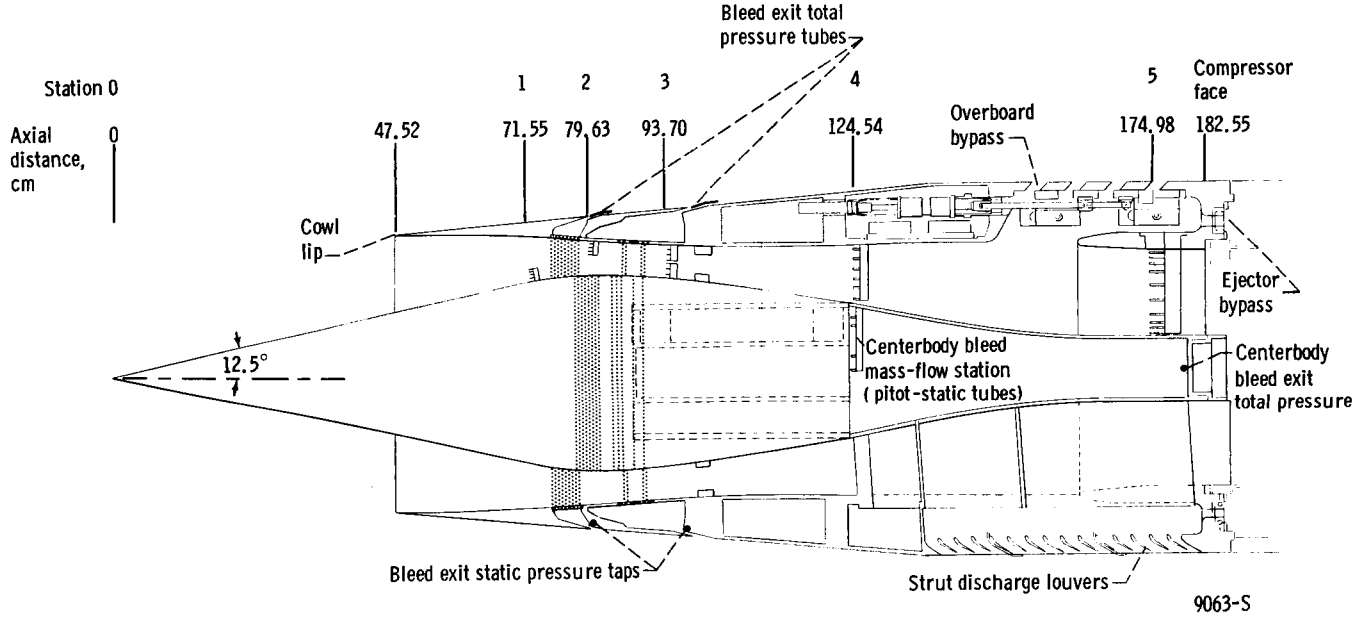


(b) Pressure instrumentation.

Figure 3. - continued.

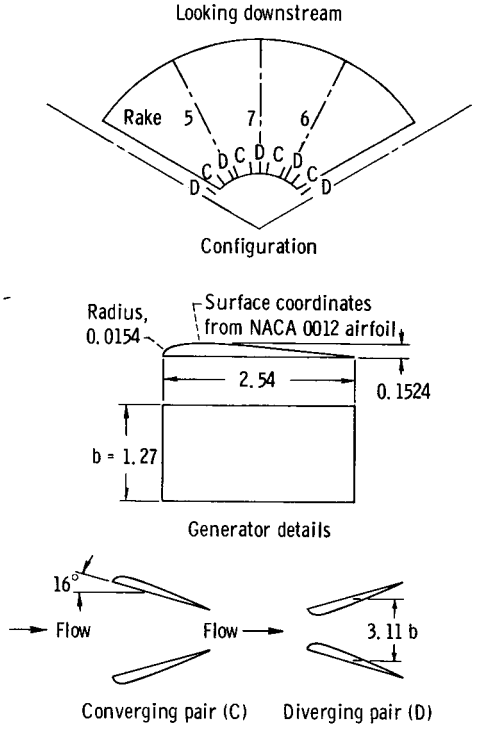


(c) Details of modified NACA 0012 airfoil vortex generator configuration. (All dimensions are in centimeters.)

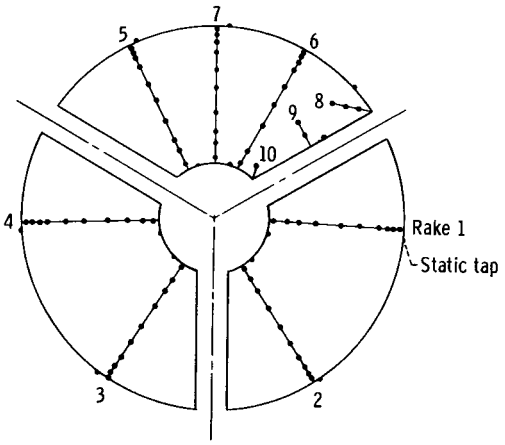


(d) Total- and static-pressure instrumentation at diffuser station 5.

Figure 3. - Concluded.

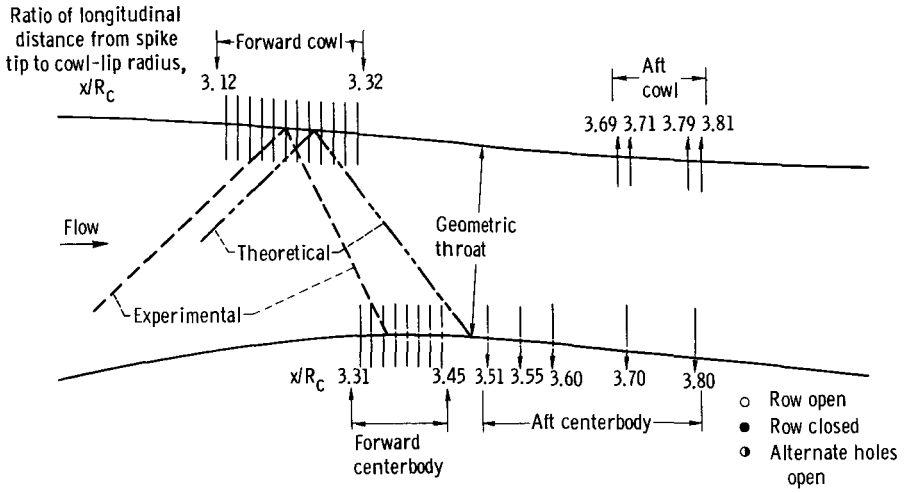


| Configuration | Forward cowl | Aft cowl | Forward centerbody | Aft centerbody |
|---|---|---|---|---|
| U. S. | ○○○○○●●●●●● | ◑● ●● | ○○○●●●●● | ◑●● ◑ ● |
| A. S. | ●●●●○○○●●●●● | ◑● ◑● | ●◑○○○●●●● | ◑◑● ◑ ● |
| D. S. and B | ●●●●●●○○●●●● | ◑● ◑● | ●●●○○○○●● | ◑◑● ◑ ● |
| A | ●●●●●●○○●●●● | ●● ●● | ●●●○○○○●● | ●●● ● ● |
| C | ●●●●○○○●●●●● | ○● ○● | ●●○○○○○○ | ○○● ◑ ◑ |
| D | ●●●●●●●○○○○○○ | ○○ ○○ | ●●●○○○○○ | ○○○ ○ ○ |

Figure 4. - Inlet bleed configurations. Bleed hole diameter, 0.3175 centimeter.

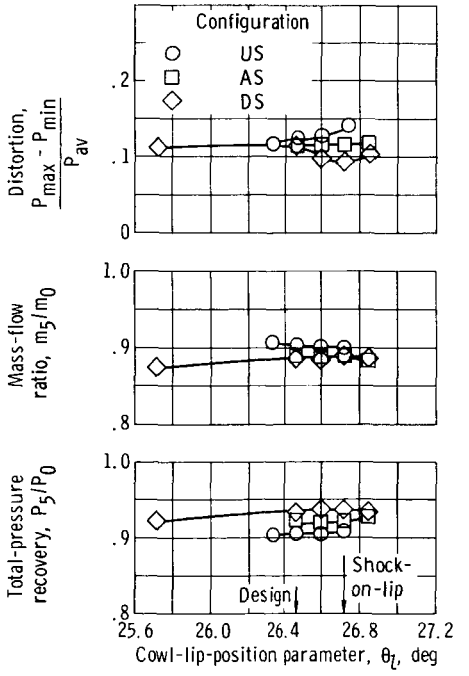


Figure 5. - Effect of spike position on peak inlet performance for various bleed locations. Angle of attack, 0°.

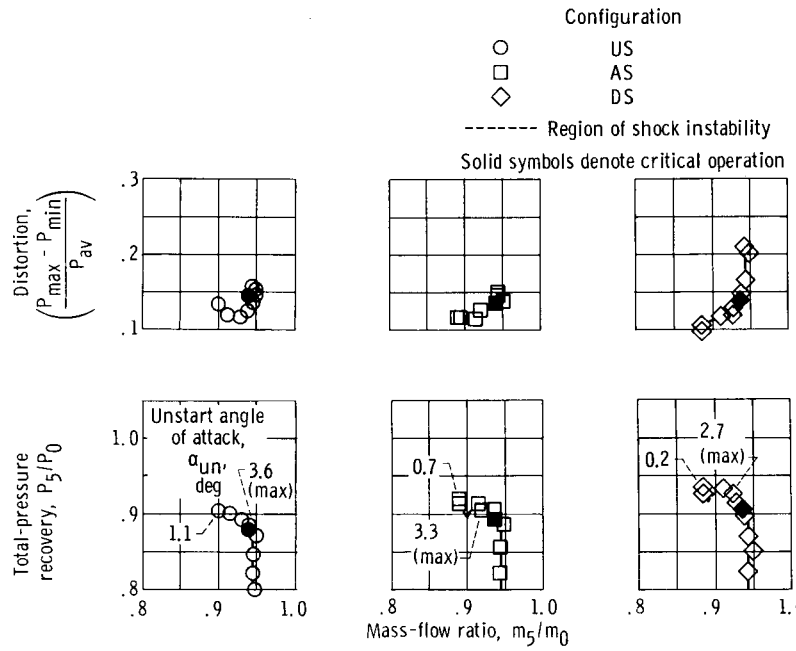


Figure 6. - Effect of bleed location on overall performance. Angle of attack; 0°; cowl-lip-position parameter, 26.6°.

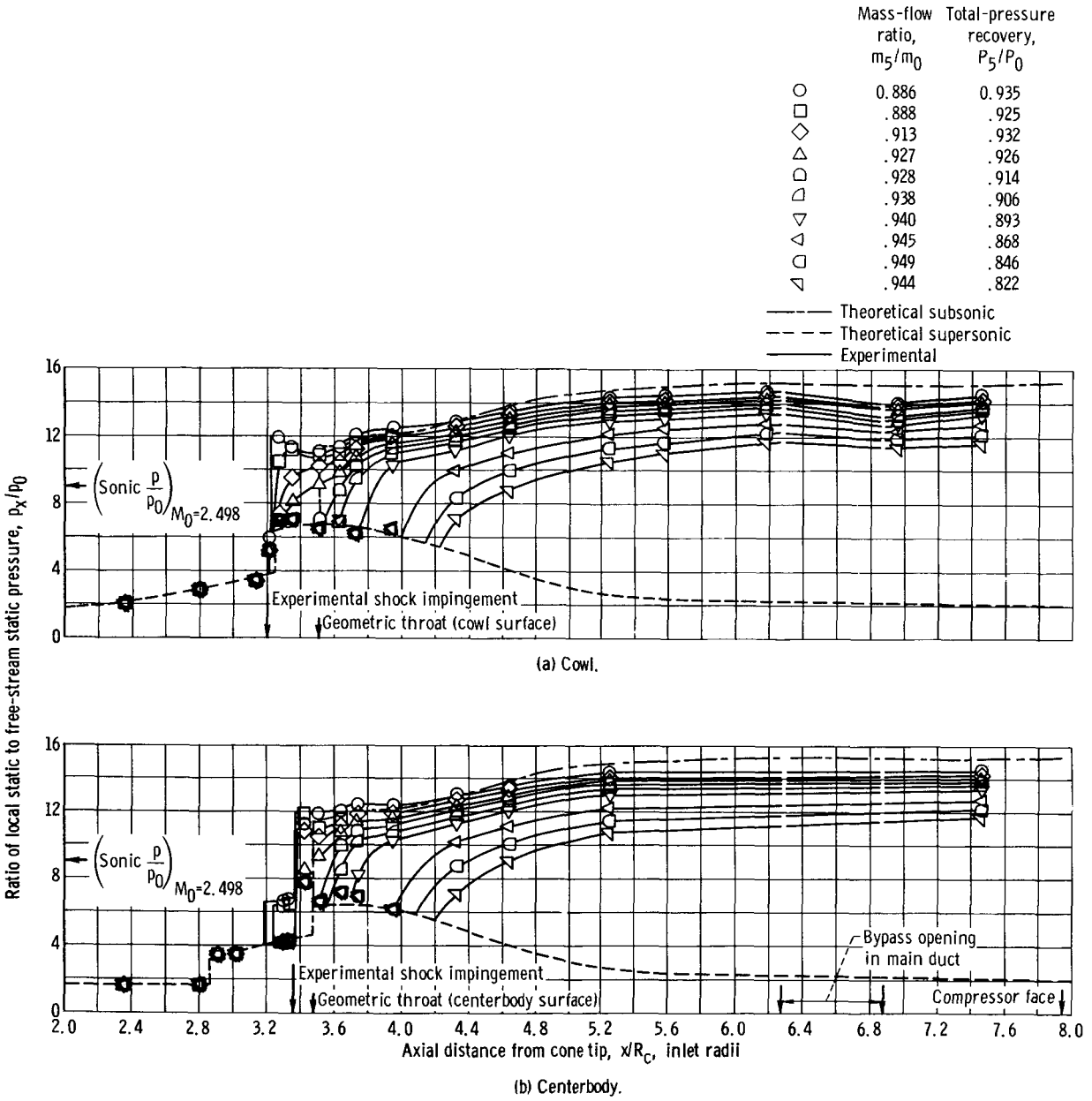


Figure 7. - Diffuser static pressure distributions for configuration DS. Mach number, 2.498; angle of attack, 0°; cowl-lip-position parameter, 26.6°.

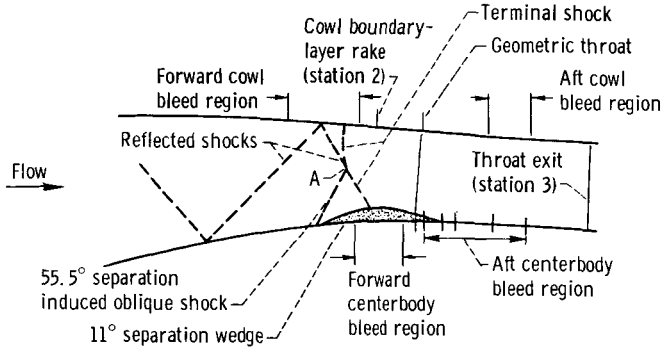


Figure 8. - Schematic of inlet shock structure caused by centerbody boundary-layer separation ahead of forward bleed.

| | Configuration | Mass-flow ratio, $m_5/m_0$ | Total-pressure recovery, $P_5/P_0$ | Distortion |
|---|---|---|---|---|
| ○ | US | 0.939 | 0.881 | 0.143 |
| □ | AS | .938 | .892 | .137 |
| ◇ | DS | .938 | .906 | .139 |

Open symbols denote total pressures
Solid symbols denote wall static pressures


Cone boundary layer, station 1

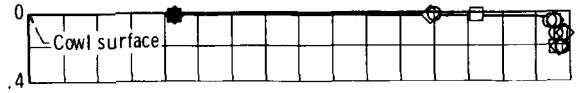


Cowl boundary layer, station 2

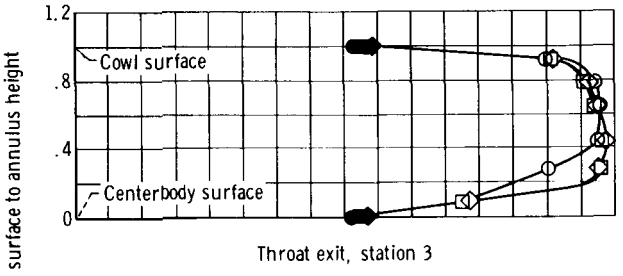


Throat exit, station 3

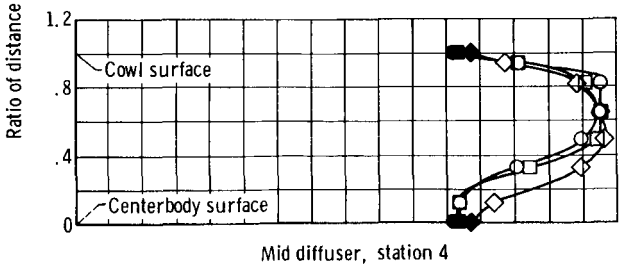


Mid diffuser, station 4

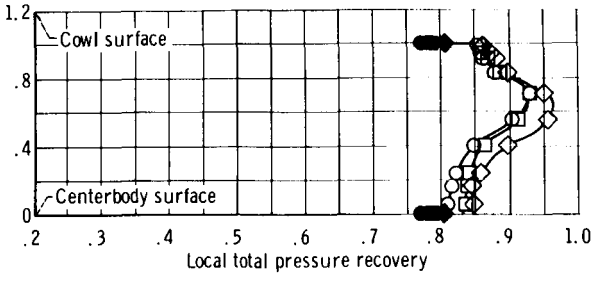


Diffuser exit, station 5, rake 7

(a) Critical inlet operating conditions.

Figure 9. - Effect of bleed location on diffuser performance. Mach number, 2.498; angle of attack, 0°; cowl-lip-position parameter, 26.6°.

| | Config-uration | Mass-flow ratio, $m_5/m_0$ | Total-pressure recovery, $P_5/P_0$ | Distor-tion |
|---|---|---|---|---|
| ○ | US | 0.900 | 0.905 | 0.132 |
| □ | AS | .889 | .920 | .118 |
| ◇ | DS | .886 | .935 | .099 |

Open symbols denote total pressure
Solid symbols denote wall static pressures

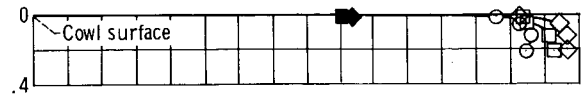


Cowl boundary layer, station 2

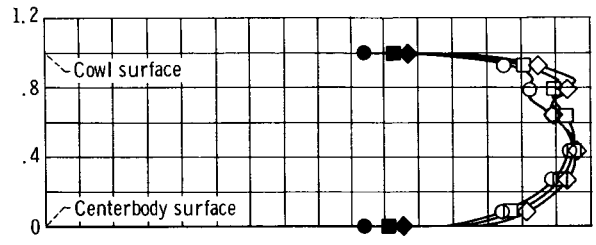


Throat exit, station 3

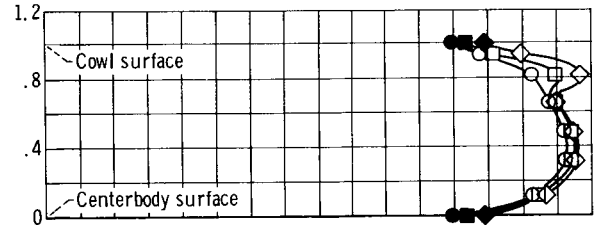


Mid diffuser, station 4

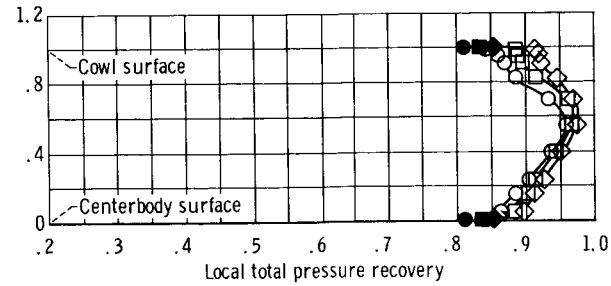


Diffuser exit, station 5, rake 7

Ratio of distance from surface to annulus height

(b) Peak inlet operating conditions.

Figure 9. - Concluded.

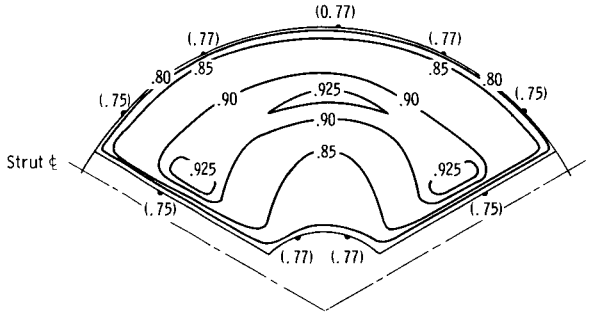


Configuration US: mass-flow ratio, 0.939; total-pressure recovery, 0.881; distortion, 0.143.

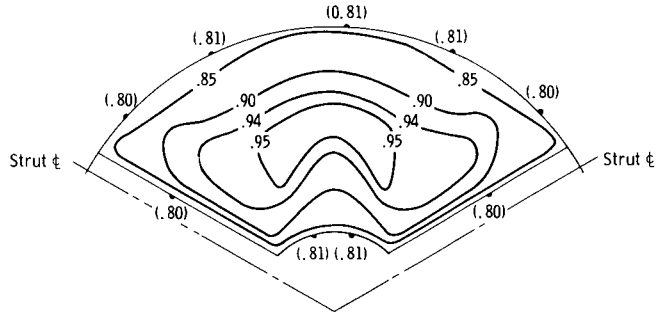


Configuration US: mass-flow ratio, 0.900; total-pressure recovery, 0.905; distortion, 0.132.

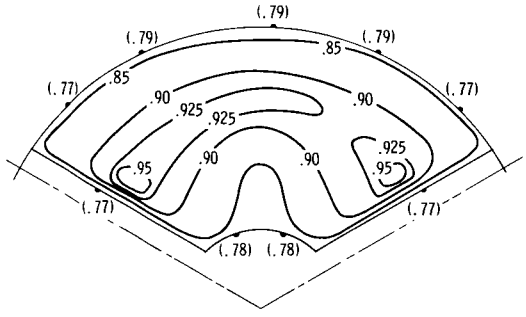


Configuration AS: mass-flow ratio, 0.938; total-pressure recovery, 0.892; distortion, 0.137.

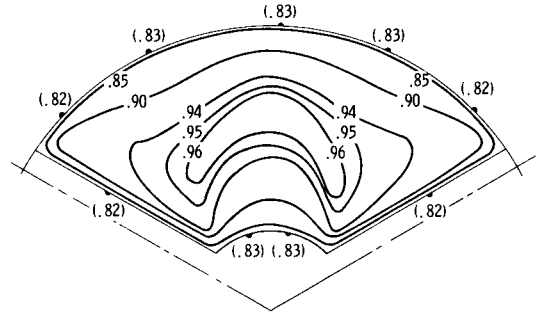


Configuration AS: mass-flow ratio, 0.889; total-pressure recovery, 0.920; distortion, 0.118.

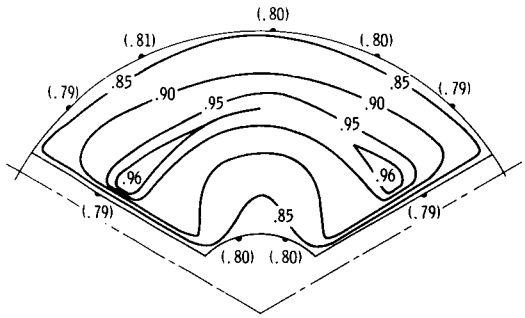


Configuration DS: mass-flow ratio, 0.938; total-pressure recovery, 0.906; distortion, 0.139.

(a) Critical inlet operating conditions.

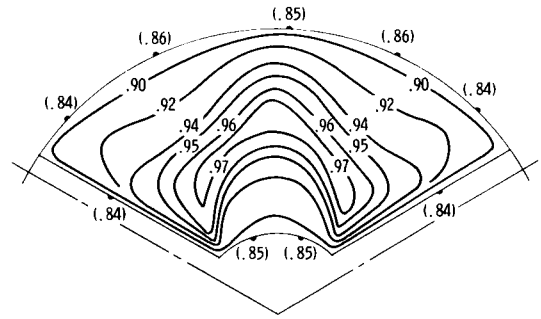


Configuration DS: mass-flow ratio, 0.886; total-pressure recovery, 0.935; distortion, 0.099.

(b) Peak inlet operating conditions.

Figure 10. - Effect of bleed location on compressor-face total-pressure maps. Angle of attack, 0°; cowl-lip-position parameter, 26.6°. (Compressor-face static-pressure ratios are given in parentheses.)

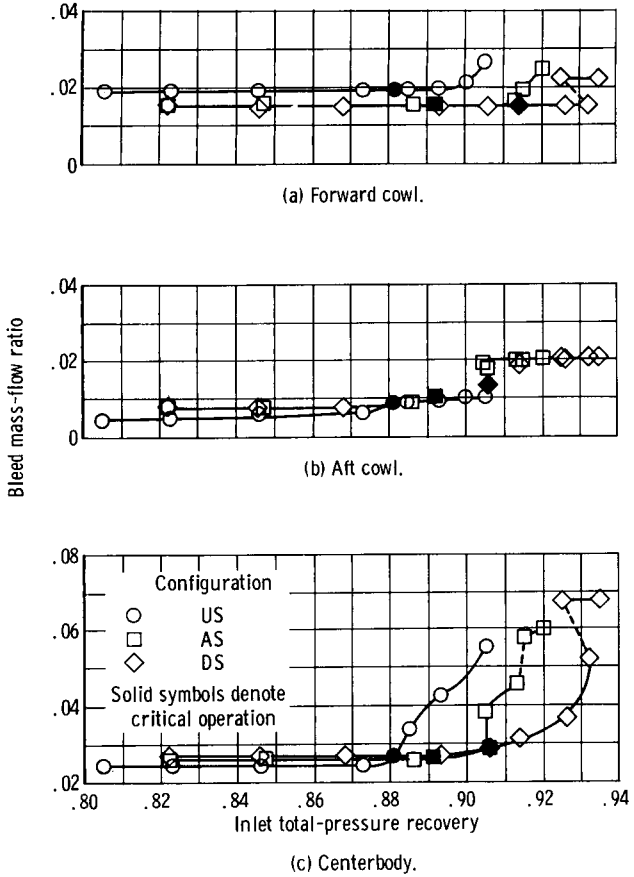


Figure 11. - Variation of bleed flow with overall inlet recovery. Angle of attack, 0°; cowl-lip-position parameter, 26.6°.

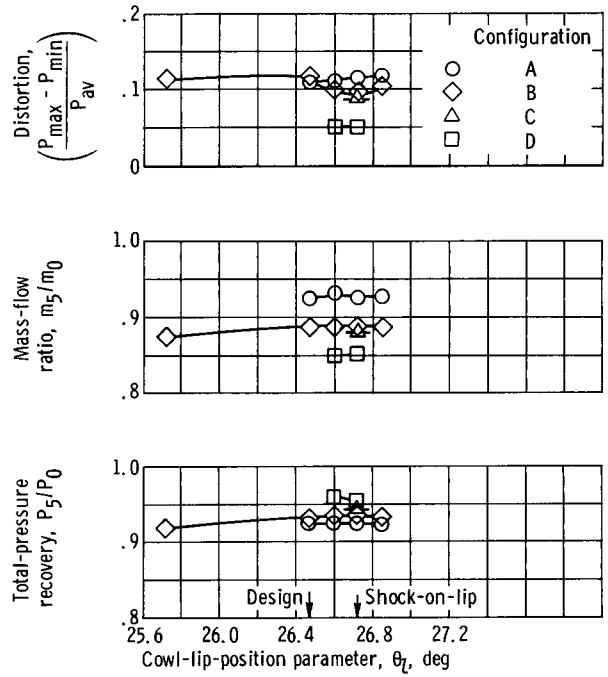


Figure 12. - Effect of spike position on peak inlet performance for various amounts of bleed. Angle of attack, 0°.

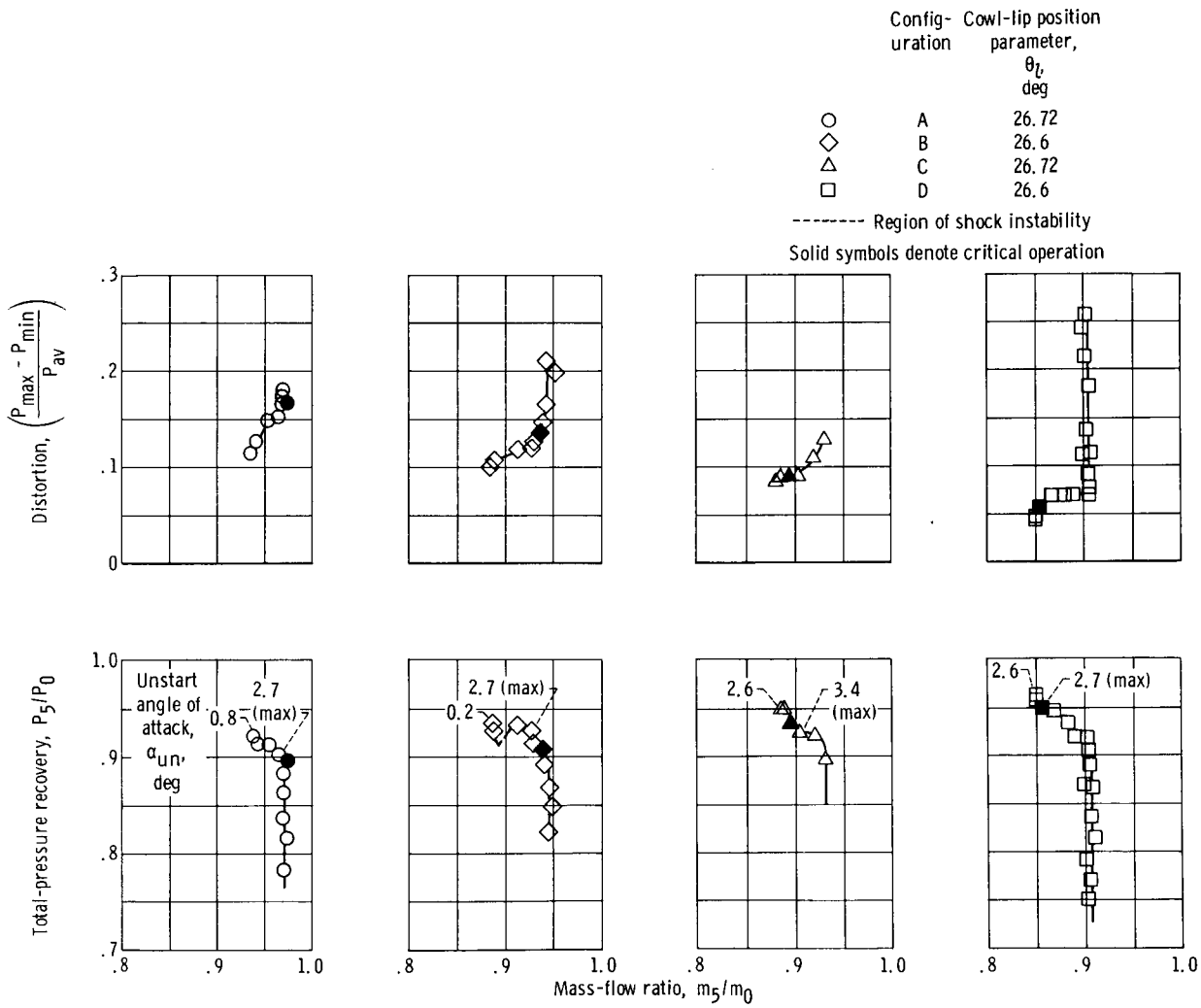


Figure 13. - Effect of the amount of bleed on overall inlet pertormance. Mach number, 2.498; angle of attack, 0°.

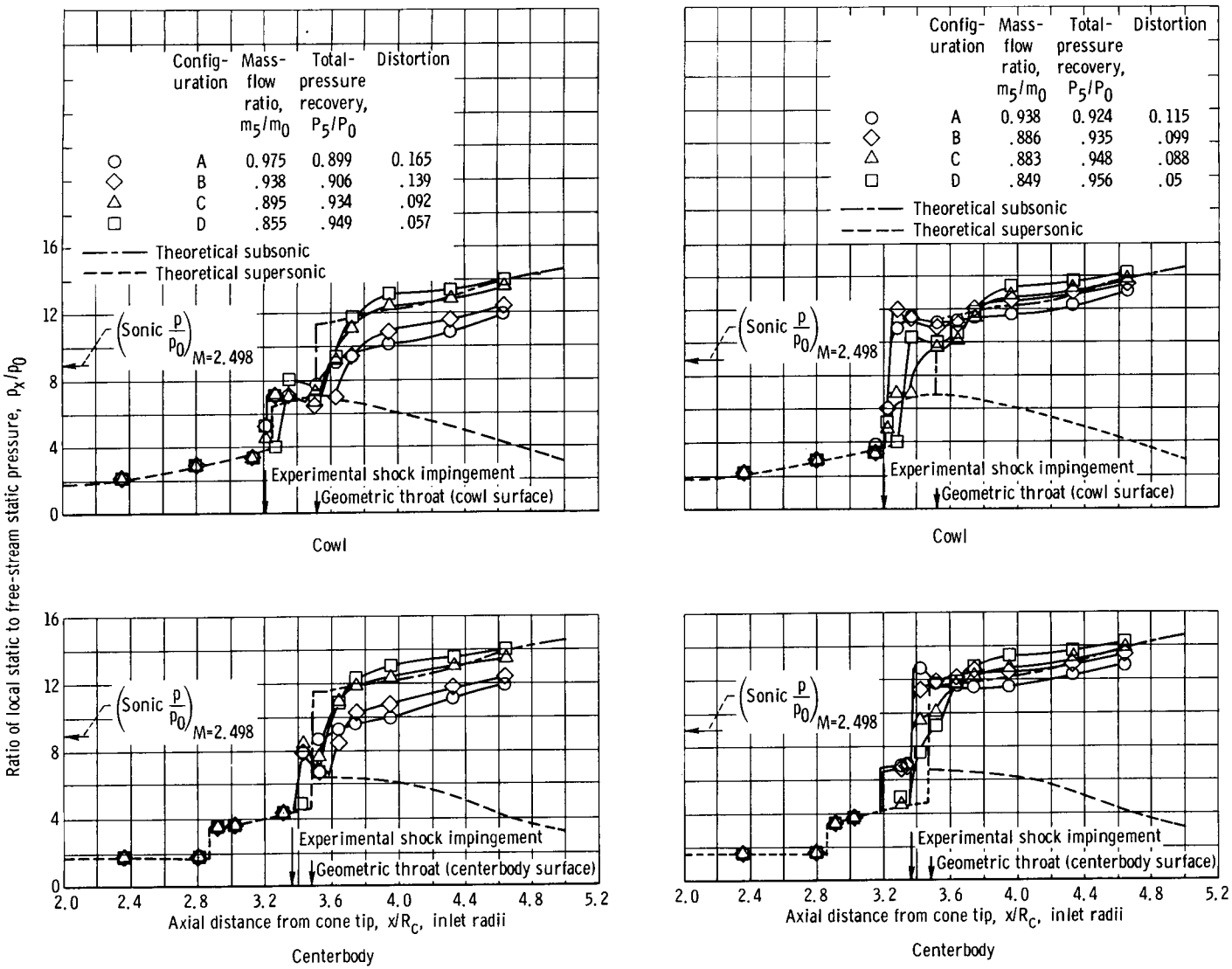


(a) Critical operation.

(b) Peak operation.

Figure 14. - Effect of the amount of bleed on the diffuser static pressure distributions. Mach number, 2.498; angle of attack, 0°.

| | Configuration | Mass-flow ratio, $m_5/m_0$ | Total-pressure recovery, $P_5/P_0$ | Distortion | Cowl-lip angle of attack, $\theta_t$, deg |
|---|---|---|---|---|---|
| ○ | A | 0.975 | 0.899 | 0.165 | 26.72 |
| ◇ | B | .938 | .906 | .139 | 26.6 |
| △ | C | .895 | .934 | .092 | 26.72 |
| □ | D | .855 | .949 | .057 | 26.6 |

Open symbols denote total pressure
Solid symbols denote wall static pressure

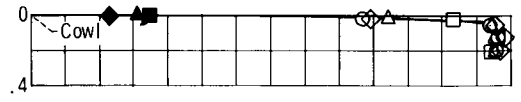


Cowl boundary layer, station 2

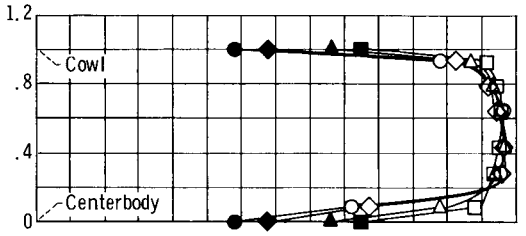


Throat exit, station 3

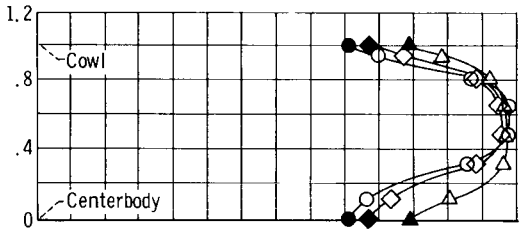


Mid diffuser, station 4

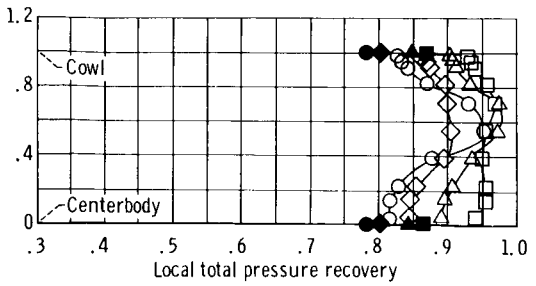


Diffuser exit, station 5, rake 7

(a) Critical inlet operating conditions.

| | Configuration | Mass-flow ratio, $m_5/m_0$ | Total-pressure recovery, $P_5/P_0$ | Distortion | Cowl-lip angle of attack, $\theta_t$, deg |
|---|---|---|---|---|---|
| ○ | A | 0.938 | 0.924 | 0.115 | 26.72 |
| ◇ | B | .886 | .935 | .099 | 26.6 |
| △ | C | .883 | .948 | .088 | 26.72 |
| □ | D | .849 | .956 | .050 | 26.6 |

Open symbols denote total pressures
Solid symbols denote wall static pressures

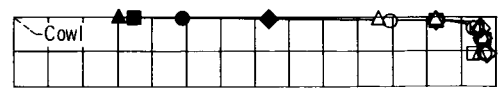


Cowl boundary layer, station 2

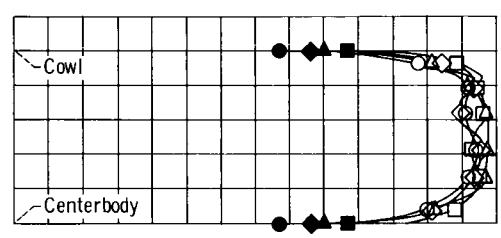


Throat exit, station 3

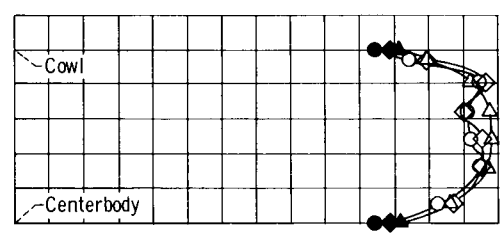


Mid diffuser, station 4

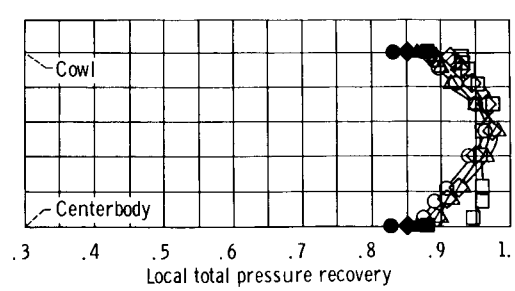


Diffuser exit, station 5, rake 7

(b) Peak inlet operating conditions.

Ratio of distance from surface to annulus height

Figure 15. - Effect of the amount of bleed on diffuser performance. Mach number, 2.498; angle of attack, 0°.

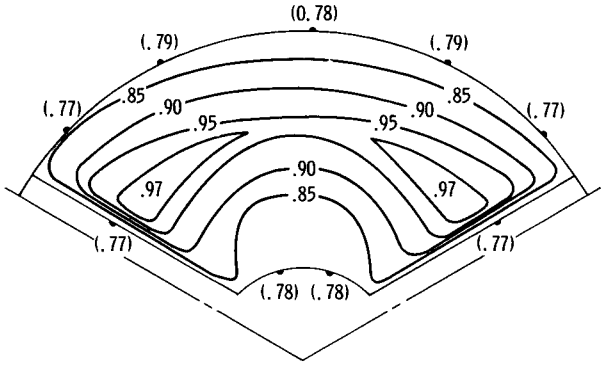


Configuration A: mass-flow ratio, 0.975; total-pressure recovery, 0.899; distortion, 0.165.

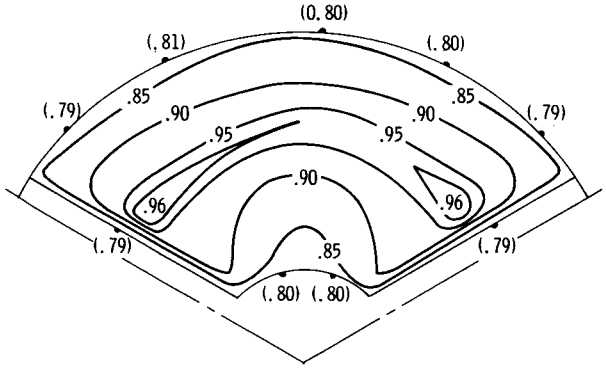


Configuration B: mass-flow ratio, 0.938; total-pressure recovery, 0.906; distortion, 0.139.

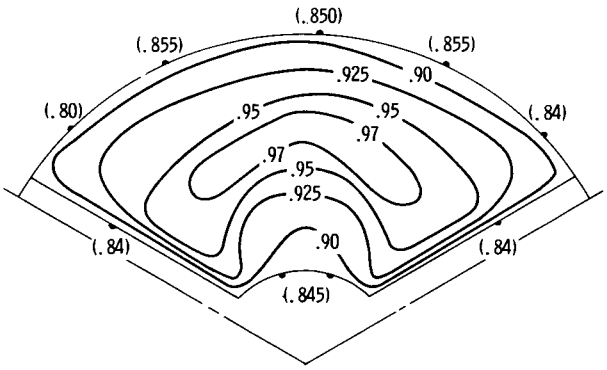


Configuration C: mass-flow ratio, 0.895; total-pressure recovery, 0.934; distortion, 0.092.

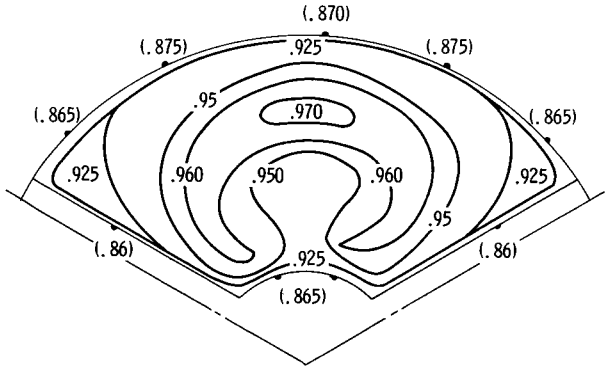


Configuration D: mass-flow ratio, 0.895; total-pressure recovery, 0.949; distortion, 0.057.

(a) Critical inlet operating condition.

Figure 16. - Effect of amount of bleed on compressor-face total-pressure maps. Angle of attack, 0°. (Compressor-face static-pressure ratios are given in parentheses.)

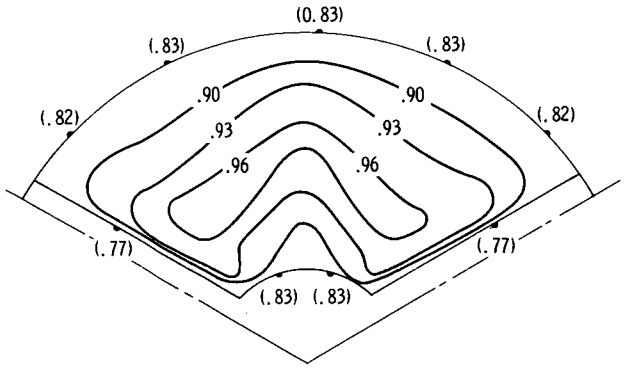


Configuration A: mass-flow ratio, 0.938; total-pressure recovery, 0.924; distortion, 0.115.

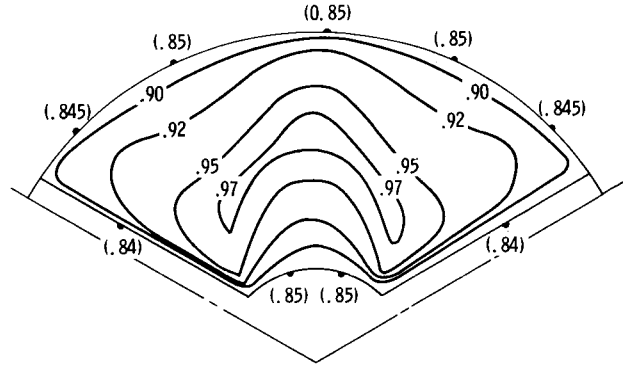


Configuration B: mass-flow ratio, 0.886; total-pressure recovery, 0.935; distortion, 0.099.

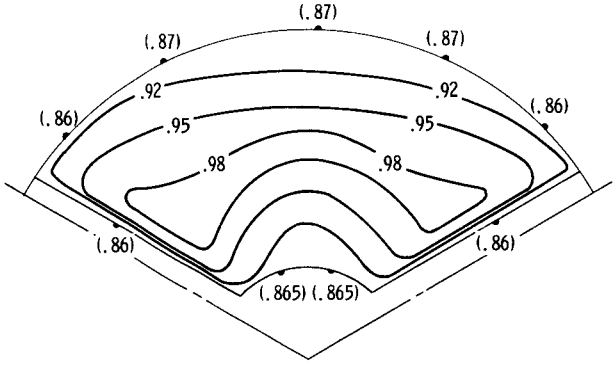


Configuration C: mass-flow ratio, 0.883; total-pressure recovery, 0.948; distortion, 0.088.

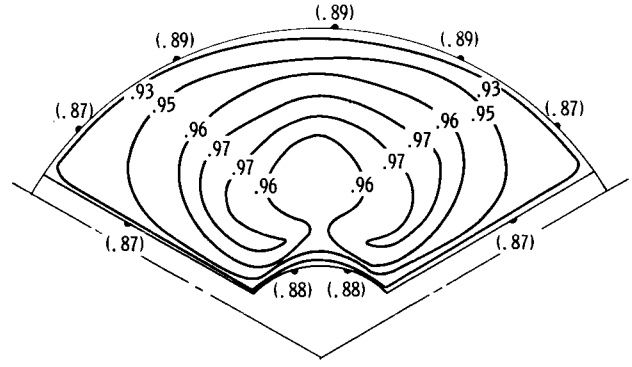


Configuration D: mass-flow ratio, 0.849; total-pressure recovery, 0.956; distortion, 0.050.

(b) Peak inlet operating conditions.

Figure 16. - Concluded.

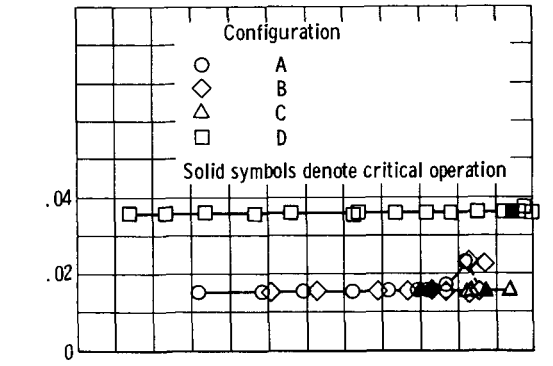


(a) Forward cowl.

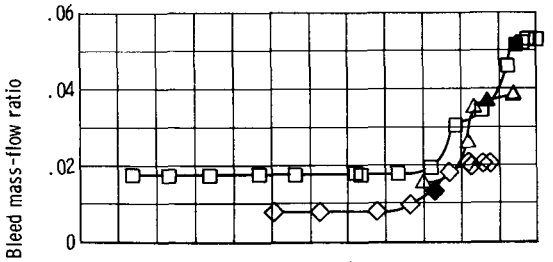


(b) Aft cowl.

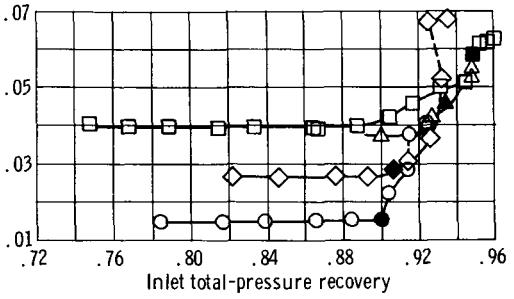


(c) Centerbody.

Figure 17. - Variation of bleed flow with overall inlet recovery. Mach number, 2.498; angle of attack, 0°.

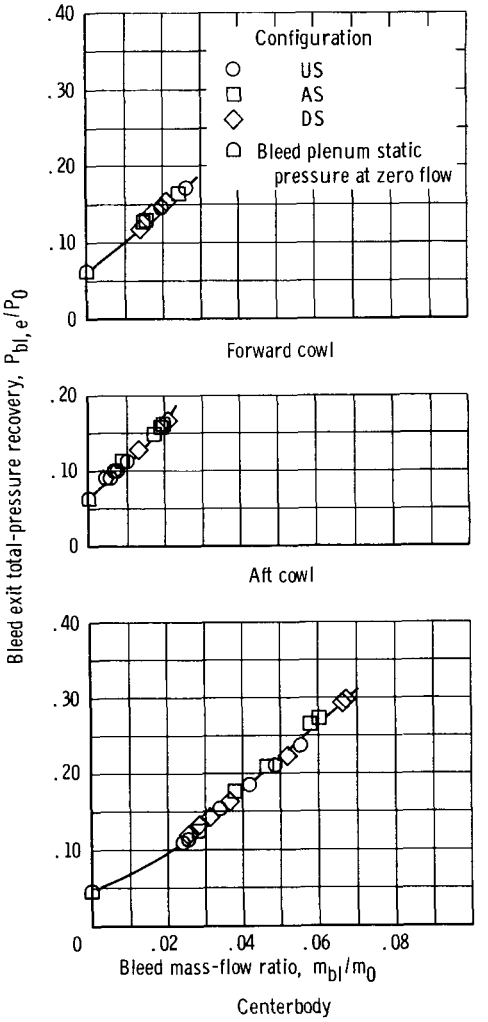


(a) Various bleed locations.

Figure 18. - Variation of bleed exit pressure recovery with bleed mass flow. Angle of attack, 0°; cowl-lip-position parameter, 26.6°.

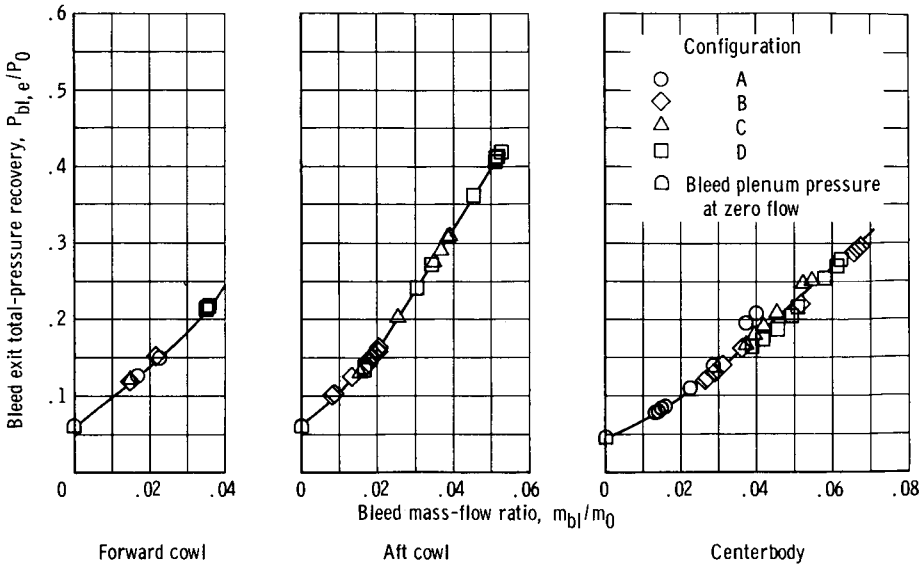


(b) Various amount of bleed.

Figure 18. - Concluded.

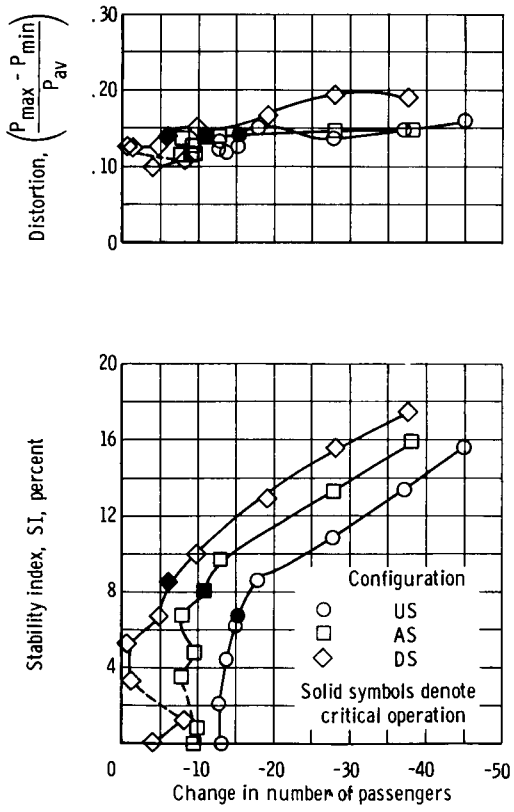


Figure 19. - Effect of bleed location on trade-offs between inlet stability and distortion in typical supersonic transport mission. Mach number, 2.498; angle of attack, 0°; cowl-lip-position parameter, 26.6°.

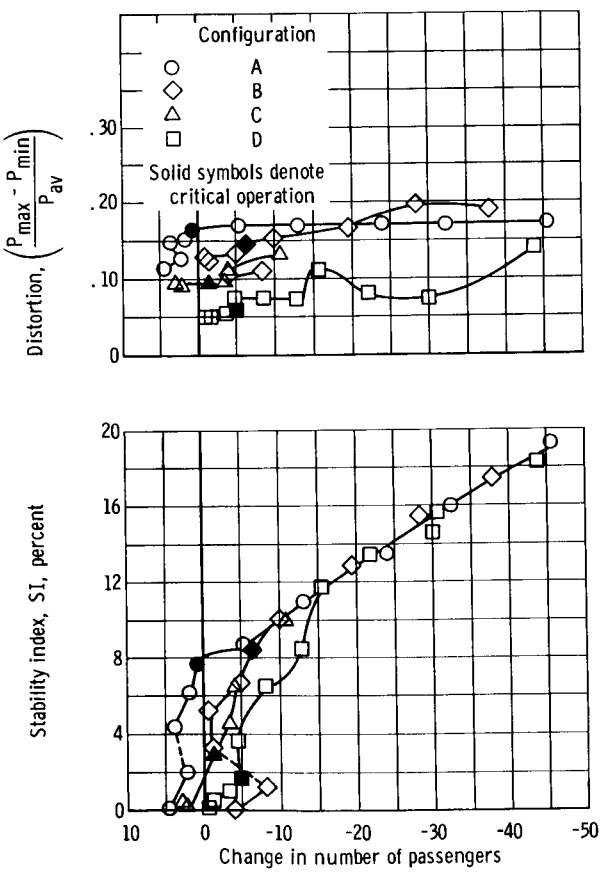


Figure 20. - Effect of amount of bleed on the trade-offs between inlet stability and distortion in typical supersonic transport mission. Mach number, 2.498; angle of attack, 0°.



NASA-Langley, 1968 — 1 E-4526